surgeries

MDPI

Article

Artificial Intelligence-Based Prediction of Surgeon Stress in Robot-Assisted Minimally Invasive Surgery Using ECG Sensor Data

Daniel Caballero [1], Manuel J. Pérez-Salazar [1], Juan A. Sánchez-Margallo [1,*] and Francisco M. Sánchez-Margallo [2]

[1] Bioengineering and Health Technologies Unit, Jesús Usón Minimally Invasive Surgery Center, Road N-521 Km. 41.8, 10071 Cáceres, Spain; dcaballero@ccmijesususon.com (D.C.); mjperez@ccmijesususon.com (M.J.P.-S.)
[2] Scientific Direction, Jesús Usón Minimally Invasive Surgery Center, Road N-521 Km. 41.8, 10071 Cáceres, Spain; msanchez@ccmijesususon.com
* Correspondence: jasanchez@ccmijesususon.com; Tel.: +34-927181032

Abstract

Background/Objectives: Robot-assisted surgery (RAS) has grown rapidly over the past few decades. To determine the effect of high stress levels on the performance of RAS, monitoring some parameters of surgeons is critical. This can be aided by the development of Artificial Intelligence (AI), which has exponentially grown in recent years. This study aims to predict the surgeon's stress level based on ergonomic, kinematic and physiological parameters of the surgeon obtained in the immediately previous situation during RAS activities. Methods: Physiological data were recorded from surgeons during twenty-six surgical sessions involving twelve participants with different levels of experience and surgical specialties. After dataset generation, two preprocessing procedures (scaling and normalization) were applied to the recorded signals. The processed data were then partitioned into two subsets: 80% of the samples were used for model training and cross-validation, while the remaining 20% were reserved for testing. Six AI approaches were evaluated to build predictive models: multiple linear regression (MLR), a support vector machine (SVM), a multilayer perceptron (MLP), a convolutional neural network (CNN), random forest (RF), and a U-Net algorithm (UNET). These algorithms were trained using the training dataset and subsequently assessed on the independent test set. In addition, after each surgical session, surgeons completed a questionnaire reporting their perceived stress level, which was later compared with the stress estimates generated by the predictive models. Results: The results obtained showed that MLR and scaling pre-processing reached the highest R^2 coefficients and the lowest error for each studied parameter. The results of the surgeons' surveys were highly correlated for microsurgery activities (R^2 = 0.7989) and for laparoscopy RAS (R^2 = 0.8381). Conclusions: The linear models proposed were correctly validated on cross-validation and the test dataset. This fact demonstrates the possibility of predicting factors that help us to improve the surgeon's health during RAS.

Keywords: minimally invasive surgery; robotic surgery; microsurgery; laparoscopy surgery; internet of things; predictive techniques; wearable devices

Check for updates

Academic Editor: Salomone Di Saverio

Received: 12 December 2025
Revised: 21 May 2026
Accepted: 30 May 2026
Published: 4 June 2026

Copyright: © 2026 by the authors. Licensee MDPI, Basel, Switzerland. This article is an open access article distributed under the terms and conditions of the Creative Commons Attribution (CC BY) license.

1. Introduction

Robotic-assisted surgery (RAS) has experienced a rapid expansion in recent years, and several robot-assisted procedures are considered standard surgical techniques [1]. The benefits of RAS for patients have previously been widely presented, and they have been clearly described in the scientific literature [2]. Among them, we may highlight the lower consumption of analgesics, the reduction in postoperative pain, shorter recovery times, or the reduction in complications derived from surgical activities. Nevertheless, despite these well-established advantages, RAS also presents important limitations for the surgeon that should be addressed, such as potential ergonomic challenges throughout prolonged surgeries and elevated stress levels in certain procedures [3], which are hazardous for the surgeon's health and have a significant impact on the quality of surgical performance and patient health care [4].

The early identification of increased stress levels may help prevent a broad spectrum of health conditions, ranging from minor illnesses such as the common cold to more serious disorders, including cardiovascular disease [5]. Because stress can affect individuals at different moments throughout their lives, developing and implementing innovative technologies capable of monitoring and managing both physiological and psychological health during everyday activities has become an important priority [6]. This need is particularly relevant in clinical environments, where stress may directly influence the quality and safety of patient care [7]. In recent years, significant technological progress has enabled the development of systems designed to assess, track, and regulate stress levels during routine activities [8] as well as during robot-assisted surgery (RAS) procedures [9].

A comprehensive evaluation of stress during RAS requires the monitoring of multiple factors, including ergonomic, kinematic, and physiological variables [10]. Within this framework, different wearable technologies have been explored to capture indicators associated with stress, among them electrocardiography (ECG) sensors used to record cardiac activity [11]. The continuous miniaturization of these devices, together with improved integration into wearable systems, has increased their suitability for monitoring surgeons' physiological condition during surgical procedures. Such technologies allow the measurement and analysis of several parameters, including ergonomic metrics as well as physiological variables such as blood pressure and body temperature [12].

In addition to this, the realization of some surgical tasks while stress levels are evaluated must be mandatory. The main tasks to measure general stress levels described in the scientific literature are: the stroop color word test, which measures cognitive flexibility, processing speed and attentional control, improving the ability to inhibit cognitive interference [13]; computer work tasks with memory demands, which measures processing speed and effect on stress levels [14]; and mental arithmetic tasks to improve processing speed [15]. The global methods to evaluate surgical skills are generally easy to implement, although they require additional training [1]. Among these tasks are peg transfers [16], cut simulation [17] and sutures on artificial models [18]. These tests have been widely used in surgery training [19]. In this study, these tests were used to measure the stress levels of the surgeons during surgery training, and the textures of artificial models could be improved to improve the realism of the tests.

In recent years, the use and development of artificial intelligence (AI) have exponentially grown at an unprecedented rate. These algorithms are based on non-trivial processes for discovering potentially useful knowledge initially hidden in the data [20]. Within the wide range of existing AI techniques, there are several algorithms specifically oriented for developing predictive models [21].

The combination of wearable technologies with AI offers considerable potential for developing novel approaches to monitor and manage surgeon stress during RAS. These technologies may also facilitate a deeper understanding of how stress levels relate to specific intraoperative situations and could support the identification or prediction of scenarios that may pose risks to the surgeon's health. In recent years, multiple studies have explored the application of AI techniques for detecting and monitoring stress across different types of activities [22]. In particular, stress assessment has been investigated both in controlled laboratory environments [23] and in real-life daily activities [8], among other contexts [19].

In current study, the applied AI techniques are focused on the linear approach (multiple linear regression—MLR) [24], the nonlinear approach (support vector machine—SVM—and random forest—RF) [25], the simplest artificial neural network (ANN) (multilayer perceptron—MLP) [26], machine learning (convolutional neural network—CNN) and deep learning architectures (U-Net Neural Network—UNET) with the aim of predicting stress levels during RAS surgery.

Therefore, the primary aim of this study is to develop predictive models capable of estimating several surgeon-related parameters during RAS, including ergonomic variables (angular rate and body posture), kinematic metrics (step count), and physiological indicators such as heart rate (beats per minute), N–N intervals, ECG signals, blood pressure, and body temperature. The proposed approach relies on previously recorded measurements to forecast the values expected in the subsequent situation, with the goal of anticipating potential health risks for the surgeon and facilitating timely interventions, such as the scheduling of rest periods.

2. Materials and Methods

2.1. Experimental Design

Data for this study were collected during twenty-six RAS sessions completed by twelve surgeons with different levels of experience, including three experts (more than one hundred surgical procedures) and three novices (less than one hundred surgical procedures) in microsurgery, as well as three experts (more than one hundred surgical procedures) and three novices (less than one hundred surgical procedures) surgeons in laparoscopy surgery. The participating surgeons were two women and ten men, aged between twenty-five and fifty years old. During the surgical procedure in both specialties, surgeons' ergonomic, kinematic, and physiological variables associated with the stress level as a function of the task accuracy, surgical task difficulty, or time required during the surgical activity were analyzed [27–29].

The data gathered are related to the ECG wearable device used in this study, including ECG signal, beats per minute, N-N intervals, blood pressure and body temperature, and the ergonomic parameters (body posture, step count, and angular rate). These measurements were recorded in the current and immediately previous situations. Based on these measurements, an initial dataset was generated, on which different pre-processing techniques (scaling and combined scaling and normalization) were applied, and two additional datasets were generated for training and cross-validation as well as for testing, with an 80–20% split, respectively. Then, six different AI techniques were applied to the training dataset to generate predictive models. Finally, the resulting models

were validated on the training (cross-validation) and independent test datasets. Data from different surgeons and surgery sessions were independently distributed across the training and test datasets, leading to more feasible performance of the AI algorithms applied in this study. Additionally, after each surgical session, a stress-sensitive survey was completed, and the survey data [30] were compared with those outputs obtained by the predictive models. For these predictive models the stress-sensitive survey was considered as the ground-truth. Figure 1 shows the experimental design adopted by this study.

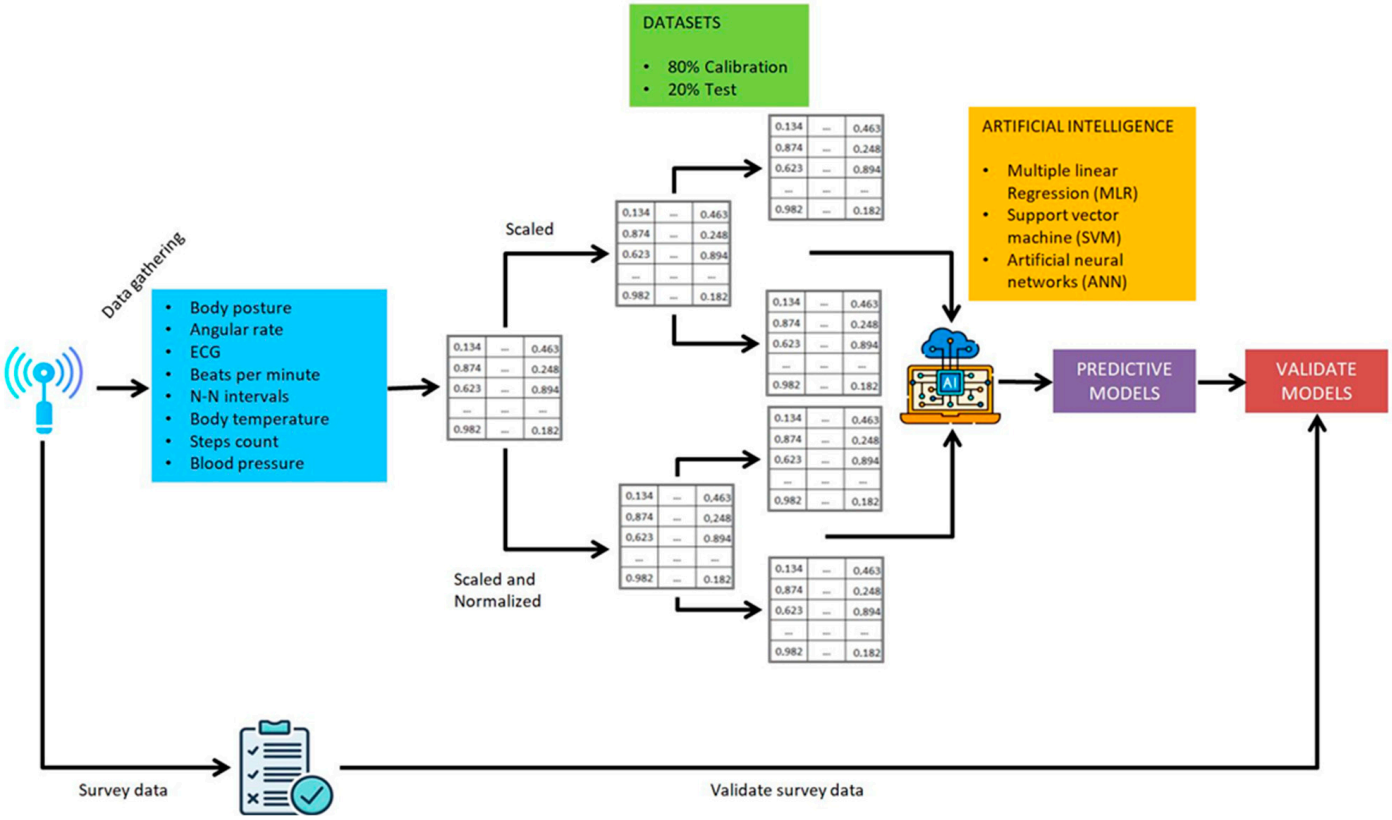

Figure 1. Workflow of the experimental study.

2.2. Clinical Setting

During the surgical procedure in both specialties, a set of predefined tasks were carried out to assess the surgeons' stress levels.

Two robotic surgical systems were utilized depending on the surgical specialty involved. For robot-assisted laparoscopic procedures, the Versius® robotic platform (CMR Surgical®, Cambridge, UK) was employed. This system is a modular robotic platform specifically developed to support laparoscopic surgery (Figure 2). It incorporates a surgeon console that enables control of the robotic instruments while providing a 3D endoscopic visualization of the operative field. On the patient side, the system can be configured with up to four independent modular robotic arms: one dedicated to the endoscopic camera and the remaining arms used to manipulate laparoscopic instruments within the patient. In total, twelve surgical sessions of robot-assisted laparoscopy were conducted using the Versius® platform.

Five tasks were performed during the surgical sessions with the Versius® robotic platform:

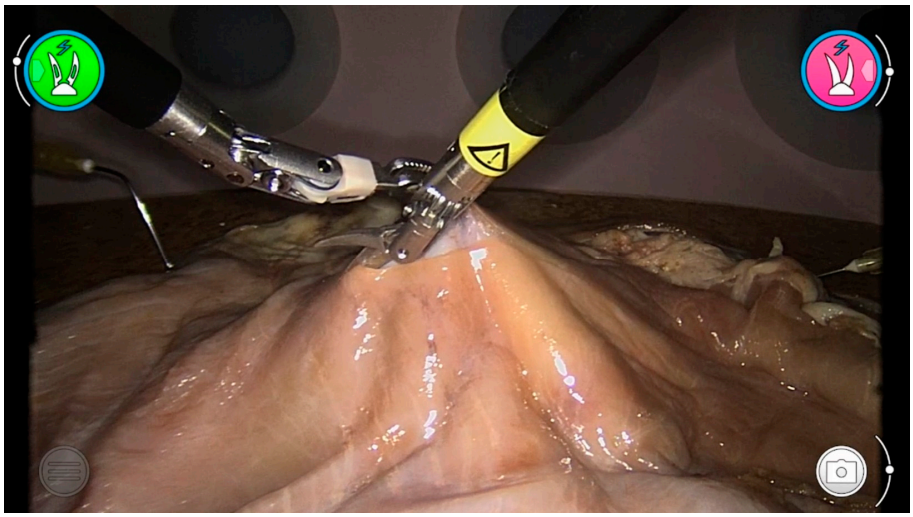

Figure 2. Stomach dissection by using the Versius® robotic surgical platform.

2.2.1. Peg Transfer

The hand–eye coordination task involved transferring rubber components with elongated toroidal shapes from one location to another while switching the object between both hands during the movement [16]. The task was performed using either two fenestrated forceps or a combination of a Maryland dissector and a fenestrated forceps. A repetition was considered completed once the three components were successfully placed in their corresponding target positions. The exercise consisted of two repetitions, with a maximum time limit of ten minutes allocated to complete both repetitions.

2.2.2. Cutting Simulation

We used the cutting template composed of two symmetrical curved lines and one circle shape. The first half of this template is cutting with the scissors in the dominant hand, while the other half of the template is performing with the non-dominant hand (the Maryland dissector was used in the other hand); each full procedure is considered one repetition. Moreover, this task was carried out with the upper horizontal line with the circumference, extracting it completely. Five minutes was the limit for each repetition (twenty minutes was the limit for the total procedure). The instrument was replaced at the beginning of each repetition.

2.2.3. Labyrinth (Needle Passing)

This task required participants to pass a needle through a sequence of holes arranged in a circuit, following a predefined order and varying directions. The purpose of the exercise was to provoke forced wrist postures in order to evaluate the surgeon's technical ability and their capacity to return to an appropriate ergonomic position [19]. During the task, the needle had to be inserted into each hole using the dominant hand and retrieved from the opposite side with the non-dominant hand. A needle holder was used in the dominant hand, while a Maryland dissector was handled with the non-dominant hand. Completion of the full circuit was considered one repetition, with a maximum time of ten minutes allocated to perform the task.

2.2.4. Stomach Dissection

An ex-vivo model was used for this task. A 3 cm long incision was created, and the surgeon had to dissect it without perforating the muscle layer. The main objective was separating the serous layer from the remaining tissue layers. Scissors were used with the dominant hand, while a Maryland dissector was used with the non-dominant hand. Only one repetition was required. Five minutes was the limit for this task.

2.2.5. Suturing

This task was performed in a synthetic training model. The goal was to perform a complete suture in a synthetic material. The suture included a needle passage, the formation of a double knot, and two additional single knots in opposite directions. A needle holder was employed in each hand. Ten minutes was the limit established for this task.

Robot-assisted microsurgical procedures were performed using the Symani® robotic system (Medical Microinstruments Inc.®, Pisa, Italy). This platform has been specifically developed to support both micro- and supermicrosurgical interventions (Figure 3). The system includes an ergonomic seating configuration for the surgeon, two robotic arms that manipulate the microinstruments, and electromagnetically tracked control interfaces used to operate the surgical tools. In addition, the platform incorporates motion scaling and tremor filtration, which improve precision when handling microsurgical instruments. As a platform for robot-assisted surgery, the level of autonomy (LoA) of this surgical robot is LoA 1. Within this study, a total of fourteen microsurgical procedures were carried out using the Symani® robotic platform.



Figure 3. Symani® robotic surgical platform.

In the case of robotic microsurgery, each surgeon performed a series of repetitions of complete anastomosis with eight stitches using synthetic vessels and the Symani® robotic platform. Each stitch consisted of (1) needle pitch; (2) double knot tying; (3) tying two simple knots. The knots had to be tied in different directions to ensure adequate closure [31]. This process was recorded for later evaluation. Three repetitions were performed, with a maximum of thirty minutes per repetition.

2.3. Wearable Device

Ergonomic and physiological variables were recorded using a wearable monitoring device (ECG Move 4® activity sensor, Movisens®, Karlsruhe, Germany). The signals obtained from the device were processed and exported using the Unisens Viewer® software (Movisens®, Karlsruhe, Germany). In addition to standard ECG measurements, the integrated sensors of the device allowed the collection of several physiological and posture-related parameters, including body temperature, heart rate, and surgeon's body position. The sensor unit was placed on the left side of the participant's torso, beneath the pectoral muscle, and secured using two electrodes (Figure 4).



Figure 4. ECG Move 4 ® activity sensor attached to the left side of the torso under the pectoral muscle.

2.4. Pre-Processing Techniques

In the current study, two pre-processing techniques were applied: scaling and normalization.

2.4.1. Scaling Pre-Processing Technique

This procedure enabled each ergonomic, kinematic and physiological parameter on a common scale between 0 and 1 [32]. For this purpose, each original value ($Value_{current}$) was transformed by subtracting the minimum value (min) and subsequently dividing by the interval between the maximum (max) and the minimum values. As a consequence, all measurements for each parameter were bounded within the interval between 0 and 1 [32].

$$Value_{new} = \frac{Value_{current} - min}{\max - min}$$

2.4.2. Normalization Pre-Processing Technique

This approach transforms the dataset into a more integrated one, with less redundancy [32]. In this case, the mean ($Value_{mean}$) was subtracted from each value ($Value_{current}$) and divided by the standard deviation ($Value_{standard\ deviation}$).

$$Value_{new} = \frac{Value_{current} - Value_{mean}}{Value_{standard\ deviation}}$$

2.5. Microsurgery Dataset

From the data acquired with the wearable device, a dataset with two thousand and sixty-four records was generated. After that, two additional datasets were derived from the original dataset by applying two pre-processing techniques: one dataset by applying scaling and the remaining one by applying combined scaling and normalization. Once

the pre-processing datasets were generated, these two datasets were divided into four different subsets: splitting eighty percent of the data for the training dataset and the cross-validation (scaling and combined scaling and normalization: one thousand six hundred and fifty-one records) and the remaining twenty percent for the test dataset (scaling and combined scaling and normalization: four hundred and thirteen records) [33].

2.6. Laparoscopy Dataset

From the data gathered by using the wearable device, a dataset with six hundred and thirty-seven records was generated. Subsequently, two datasets were achieved from the original dataset by applying two pre-processing techniques: one dataset by applying scaling and the remaining one by applying scaling and normalization. These two datasets were divided into four different subsets, splitting eighty percent of the data for the training dataset and the cross-validation (scaling and combined scaling and normalization: five hundred and ten records) and the remaining twenty percent for the test dataset (scaling and combined scaling and normalization: one hundred and twenty-seven records) [33].

2.7. Artificial Intelligence

The free open-source software WEKA® v 3.8.6 (Waikato Environment for Knowledge Analysis) (University of Waikato, Hamilton, New Zealand) [34] was employed for the development of the predictive models. Six different AI predictive techniques (convolutional neural network—CNN, multilayer perceptron—MLP, multiple linear regression—MLR, random forest—RF, support vector machine—SVM, and U-Net Neural Network—UNET) were applied to the training dataset to build predictive models. Finally, to validate the performance of the generated models, they were assessed in ten-fold cross-validation, in which the training dataset was divided into ten equally sized partitions. Each time a subset was tested, while the remaining data were used to fit the model. The process was repeated sequentially until all subsets were tested. Therefore, all data were used for training and validation. Although this method requires ten cycles of analysis, it is a good validation strategy [35]. Finally, the independent test dataset was used to perform an external validation of the predictive models.

2.7.1. Convolutional Neural Network (CNN)

A CNN was implemented as a machine learning representation. A CNN is a type of machine learning algorithm that is particularly suitable for processing grid-like data, such as images or matrix data [36]. It is particularly effective in computer vision and pattern recognition tasks because it can automatically learn and extract relevant hierarchical feature representations directly from the input data. The architecture followed by our CNN consists of: a first convolutional layer, a first max-pooling layer, a second convolutional layer, a second max-pooling layer and the fully connected layer by ReLU activation. The applied configuration was as follows: learning rate: 0.3, number of epochs: 500 and momentum: 0.1.

2.7.2. Multilayer Perceptron (MLP)

An MLP was applied as a predictive machine learning approach. MLPs belong to a family of ANN models that are inspired by principles of neuronal organization [37]. In this architecture, different numbers of neurons were aggregated into multiple layers. Different layers may perform specific transformations on their inputs. A signal travels throughout the network by successively traversing the layers [38]. The configuration used in the current study was as follows [39]: learning rate: 0.3, number of epochs: 500, momentum: 0.1, threshold: 20, nodes in the first hidden layer: 30, nodes in the second hidden layer: 10, nodes in the third hidden layer: 3.

2.7.3. Multiple Linear Regression (MLR)

Predictive techniques enable the construction of future models that can be predicted from current observations through trend analysis [40]. MLR was adopted as a predictive linear approach. MLR was performed, showing the linear relationship between a dependent variable and several independents' variables. This technique reaches a linear regression equation that can be used to estimate future values.

For attribute selection, the M5 method was applied in this study [41]. This method steps iteratively through the attributes, removing the one with the smallest standardized coefficient until no improvement in the estimation of the error is observed. A ridge value of 1.0×10^{-4} was applied too [41].

$$y = \sum_{i=1}^{n} \omega_i \cdot x_i$$

2.7.4. Random Forest (RF)

RF is a powerful ensemble-based machine learning algorithm that combines an ensemble of decision trees to construct predictive models [42]. RF is particularly known for its ability to handle complex or high-dimensional data to reach a single result that combines the mean of the output of multiple decision trees, improving performance. The hyperparameters for RF are: number max of trees: 20, maxDepth: 0, numSlots: 1 and numIterations: 100.

2.7.5. Support Vector Machine (SVM)

An SVM was employed as a predictive non-linear approach. The SVM was employed to represent desirable non-linear relationship models by finding the optimal decision that minimizes the separation, tolerating the smallest error when fitting the data in the transformed feature space [43].

$$y = \omega_0 \cdot \sum_{i=1}^{n} \omega_i \cdot K_i(x)$$

To enable this transformation into a high-dimensional feature space, a non-linear mapping without the need to be explicitly known but depending on a kernel function was used [43]. The kernel function computes the inner product of the feature space. Among the most frequently used kernel functions are the polynomial function, the radial basis function (RBF) and the sigmoid function. In the current study, the RBF was used as a kernel function.

$$K(u, v) = \exp(-\gamma \cdot |u - v|)^2$$

2.7.6. U-Net Neural Network (UNET)

The UNET is a deep learning architecture applied primarily to image segmentation, especially in biomedical images. It is characterized by using two symmetric processing paths to generate predictive models, one initial path to contract the model (encoder), which progressively captures contextual information and reduces the spatial resolution, and the use of another final path to expand the model (decoder), which restores the spatial resolution to produce detailed predictions [44]. This architecture is highly feasible for obtaining spatial information on matrix-structured data or for performing accurate image and spatial segmentation tasks. The applied configuration was as follows: learning rate: 0.3, number of epochs: 500 and momentum: 0.1.

2.7.7. Evaluation Metrics

The coefficient of determination (R^2) was employed to assess the goodness of fit of the predictive models and to support their validation, following the classification proposed

by Colton [45]. According to this criterion, R^2 values between 0 and 0.25 indicate little or no relationship; values from 0.25 to 0.50 correspond to a weak association; values between 0.50 and 0.75 reflect a moderate to good relationship; and values ranging from 0.75 to 1.00 represent a very good to excellent level of association.

$$R^2 = \frac{\sum_{i=1}^{n}(f_i - \overline{y})^2}{\sum_{i=1}^{n}(y_i - \overline{y})^2}$$

The root mean square error (*RMSE*) was also employed to validate the performance of the prediction results. The *RMSE* quantifies the difference between actual values and the corresponding prediction ones. *RMSE* values less than 0.05 were considered appropriate and indicative of satisfactory accuracy [46].

$$RMSE = \sqrt{\frac{1}{n} \cdot \sum_{i=1}^{n}(f_i - y_i)^2}$$

2.8. Statistical Analysis

Predicted and measured values of the physiological and kinematic parameters of the ECG sensor were compared by using one-way analysis of variance (ANOVA) using the general linear model procedure. The statistical analyses were performed by using the SPSS (v 21.0) package software.

3. Results

Table 1 summarizes the results obtained for the training dataset for the robot-assisted microsurgery sessions performed by Symani® surgical platform (Medical Microinstruments Inc.®). This table reports the values of R^2 and RMSE for the predictive analysis carried out by applying the CNN, MLP, MLR, RF, SVM and UNET as AI techniques, with the datasets pre-processed by scaling and combined scaling and normalization. The combination of MLR as a predictive technique and scaling as a pre-processing technique yielded the highest values of the R^2 coefficient and lowest values of the RMSE, followed by the SVM, RF, MLP, CNN and UNET.

Overall, the results achieved on the training dataset are considered satisfactory according to the criteria proposed by Colton [45]. High to excellent correlations were achieved, close to 1 ($R^2 > 0.75$) and RMSE close to 0 (RMSE < 0.05) for the body posture on the X, Y and Z coordinates; angular rate on the Y axis; ECG signal; beats per minute; N-N intervals; step count; blood pressure and body temperature. Particularly noteworthy results were the R^2 coefficient values for blood pressure ($R^2 = 0.9987$ and RMSE = 0.0014) and body temperature ($R^2 = 0.9912$ and RMSE = 0.0051). A low to good relationship ($R^2 > 0.25$ and $R^2 < 0.75$) was observed for the angular rate along the X and Z axes. No statistically significant differences were found in any of the analyzed cases ($p > 0.05$).

The results obtained from the cross-validation analysis of the robot-assisted microsurgery sessions performed by using the Symani® robotic surgical platform are presented in Table 2. This table shows the values of the R^2 coefficient and RMSE for the cross-validation analysis conducted by applying the CNN, MLP, MLR, RF, SVM, and UNET as AI techniques, all of them with data pre-processed by scaling and combined scaling and normalization techniques. The best performance of the predictive analysis was achieved by MLR as an AI technique and scaling as a pre-processing technique, achieving the highest values of the R^2 coefficient and the lowest RMSE values followed in descending order of performance by the SVM, RF, MLP, CNN and UNET.

Table 1. Results of the R^2 coefficient and RMSE for the training dataset of the ECG parameters as a function of the predictive techniques (CNN, MLP, MLR, RF, SVM and UNET) and the pre-processing techniques (scaling and combined scaling and normalization) by using the Symani® robotic surgical platform. The best results are highlighted in bold.

		MLP		MLR		SVM		CNN		RF		UNET	
		Scaling	Scaling and Normalization	Scaling	Scaling and Normalization	Scaling	Scaling and Normalization	Scaling	Scaling and Normalization	Scaling	Scaling and Normalization	Scaling	Scaling and Normalization
Body posture X	R^2	0.8293	0.8292	**0.8843**	0.8631	0.8419	0.8418	0.6393	0.6342	0.8393	0.8342	0.4393	0.4342
	RMSE	0.0461	0.3093	**0.0315**	0.2501	0.0372	0.2791	0.1314	0.3953	0.0431	0.2953	0.3314	0.5953
Body posture Y	R^2	0.8276	0.8274	**0.8755**	0.8676	0.8613	0.8611	0.6376	0.6471	0.8376	0.8471	0.4376	0.4471
	RMSE	0.0409	0.3489	**0.0282**	0.3031	0.0364	0.3109	0.1933	0.4189	0.0393	0.3298	0.3933	0.6189
Body posture Z	R^2	0.9454	0.9453	**0.9573**	0.9569	0.9568	0.9567	0.6534	0.6532	0.9534	0.9532	0.4534	0.4532
	RMSE	0.0407	0.1827	**0.0334**	0.1531	0.0354	0.1687	0.1777	0.2719	0.0377	0.1729	0.3777	0.4719
Angular rate X	R^2	0.5336	0.5335	**0.5398**	0.5396	0.5306	0.5302	0.3356	0.3355	0.5356	0.5355	0.1356	0.1355
	RMSE	0.0351	0.5292	**0.0251**	0.4401	0.0292	0.6354	0.1301	0.6152	0.0311	0.5122	0.3301	0.8152
Angular rate Y	R^2	0.6582	0.6581	**0.7625**	0.7623	0.7378	0.7367	0.4862	0.4814	0.6862	0.6814	0.2862	0.2814
	RMSE	0.0413	0.6354	**0.0344**	0.5282	0.0379	0.5505	0.1204	0.7416	0.0402	0.6421	0.3204	0.9416
Angular rate Z	R^2	0.5286	0.5284	**0.5604**	0.5601	0.5581	0.5517	0.3286	0.3284	0.5286	0.5284	0.1286	0.1284
	RMSE	0.0228	0.6087	**0.0166**	0.4443	0.0188	0.4947	0.0902	0.6784	0.0209	0.5874	0.2902	0.8784
ECG signal	R^2	0.6112	0.6111	**0.7559**	0.7557	0.6761	0.6869	0.4412	0.4411	0.6412	0.6411	0.2412	0.2411
	RMSE	0.0147	0.4826	**0.0113**	0.3206	0.0132	0.4272	0.1371	0.5462	0.0137	0.4542	0.3371	0.7462
Beats per minute	R^2	0.7498	0.7497	**0.7859**	0.7858	0.7842	0.7841	0.6682	0.6579	0.7682	0.7579	0.4682	0.4579
	RMSE	0.0509	0.4144	**0.0341**	0.3385	0.0419	0.3422	0.1294	0.4924	0.0492	0.3944	0.3294	0.6924
N-N intervals	R^2	0.8064	0.8061	**0.8302**	0.8297	0.8224	0.8223	0.6164	0.6165	0.8164	0.8165	0.4164	0.4165
	RMSE	0.0752	0.4109	**0.0449**	0.3565	0.0617	0.3698	0.1567	0.4991	0.0657	0.3909	0.3567	0.6991
Step count	R^2	0.5763	0.5574	**0.7866**	0.7667	0.6972	0.6963	0.4354	0.3977	0.6354	0.5977	0.2354	0.1977
	RMSE	0.1278	0.6055	**0.0475**	0.3148	0.0815	0.3799	0.1971	0.7061	0.1079	0.5035	0.3971	0.9061
Blood pressure	R^2	0.9973	0.9929	**0.9987**	0.9955	0.9982	0.9952	0.6976	0.6936	0.9976	0.9936	0.4976	0.4936
	RMSE	0.0021	0.0098	**0.0014**	0.0072	0.0018	0.0077	0.1109	0.1094	0.0019	0.0089	0.3109	0.3094
Body temperature	R^2	0.9845	0.9389	**0.9912**	0.9661	0.9901	0.9653	0.6885	0.6593	0.9885	0.9593	0.4885	0.4593
	RMSE	0.0128	0.0518	**0.0051**	0.0208	0.0084	0.0234	0.1201	0.1182	0.0102	0.0318	0.3201	0.3182

Table 2. Results of the R^2 coefficient and RMSE for the cross-validation analysis of the ECG parameters as a function of the predictive techniques (CNN, MLP, MLR, RF, SVM, and UNET) and the pre-processing techniques (scaling and combined scaling and normalization) by using the Symani® robotic surgical platform. The best results are highlighted in bold.

		MLP		MLR		SVM		CNN		RF		UNET	
		Scaling	Scaling and Normalization	Scaling	Scaling and Normalization	Scaling	Scaling and Normalization	Scaling	Scaling and Normalization	Scaling	Scaling and Normalization	Scaling	Scaling and Normalization
Body posture X	R^2	0.8135	0.8131	**0.8407**	0.8405	0.8305	0.8257	0.6351	0.6275	0.8253	0.8231	0.4316	0.4258
	RMSE	0.0856	0.5756	**0.0421**	0.2828	0.0602	0.3846	0.4621	0.7864	0.0756	0.5656	0.6622	0.9865
Body posture Y	R^2	0.7527	0.7519	**0.8628**	0.8616	0.8371	0.8364	0.6317	0.6346	0.7725	0.7792	0.4318	0.4347
	RMSE	0.0835	0.7134	**0.0363**	0.3101	0.0651	0.3514	0.4615	0.7541	0.0735	0.7034	0.6616	0.9542
Body posture Z	R^2	0.9426	0.9416	**0.9543**	0.9539	0.9482	0.9456	0.6428	0.6465	0.9462	0.9436	0.4429	0.4466
	RMSE	0.0733	0.3287	**0.0373**	0.1671	0.0647	0.2904	0.5674	0.7941	0.0633	0.3187	0.7675	0.9942
Angular rate X	R^2	0.5164	0.5162	**0.5251**	0.5248	0.5154	0.5092	0.3145	0.3029	0.5174	0.5182	0.1146	0.1030
	RMSE	0.1361	1.1302	**0.0284**	0.4291	0.0723	1.0929	0.4732	1.4992	0.1261	1.1202	0.8733	1.8993
Angular rate Y	R^2	0.6455	0.6451	**0.7226**	0.7218	0.7018	0.6939	0.5081	0.4993	0.6755	0.6651	0.3082	0.2994
	RMSE	0.0891	0.6972	**0.0352**	0.5414	0.0685	0.6119	0.4658	1.0191	0.0791	0.6772	0.6659	1.2192
Angular rate Z	R^2	0.5281	0.4719	**0.5414**	0.5289	0.5318	0.5064	0.3381	0.3046	0.5293	0.4917	0.1382	0.1047
	RMSE	0.0631	0.6308	**0.0159**	0.4257	0.0412	0.4988	0.4421	0.8988	0.0531	0.6108	0.6422	1.0989
ECG signal	R^2	0.5581	0.5578	**0.7303**	0.7296	0.6394	0.6244	0.4349	0.4244	0.5816	0.5783	0.2350	0.2245
	RMSE	0.0399	0.5528	**0.0111**	0.3616	0.0322	0.4263	0.4322	0.8236	0.0358	0.4524	0.6323	1.0237
Beats per minute	R^2	0.6907	0.6904	**0.7841**	0.7838	0.7783	0.7778	0.5738	0.5787	0.7072	0.7043	0.3739	0.3788
	RMSE	0.1069	0.8727	**0.0445**	0.3629	0.0838	0.4394	0.4883	0.8349	0.0916	0.8622	0.6884	0.6350
N-N intervals	R^2	0.7661	0.7653	**0.8288**	0.8284	0.8129	0.8128	0.6192	0.6182	0.7861	0.7853	0.4193	0.4183
	RMSE	0.0906	0.7329	**0.0443**	0.3582	0.0716	0.3799	0.4761	0.7799	0.0816	0.7293	0.6762	0.9800
Step count	R^2	0.6536	0.6527	**0.7766**	0.7664	0.6911	0.6909	0.4911	0.4991	0.6738	0.6729	0.2912	0.2992
	RMSE	0.1112	0.9701	**0.0478**	0.4169	0.0986	0.4808	0.4968	0.8881	0.1211	0.9801	0.6969	0.8881
Blood pressure	R^2	0.9966	0.9882	**0.9981**	0.9955	0.9978	0.9948	0.6987	0.6984	0.9976	0.9927	0.4987	0.4985
	RMSE	0.0025	0.0089	**0.0013**	0.0027	0.0015	0.0061	0.5051	0.5016	0.0019	0.0078	0.7052	0.7017
Body temperature	R^2	0.9905	0.9536	**0.9942**	0.9609	0.9935	0.9562	0.6953	0.6526	0.9917	0.9554	0.4954	0.4527
	RMSE	0.0061	0.0244	**0.0032**	0.0211	0.0058	0.0235	0.5085	0.5253	0.0060	0.0241	0.7086	0.7254

As expected, the cross-validation results reached lower values than those obtained with the training dataset since the training dataset was divided into ten subsets, and nine of them were used to generate the predictive models, and the remaining one was used to validate the generated models. Nevertheless, the results obtained were considered successful as far as the training dataset is concerned.

High to excellent correlations ($R^2 > 0.75$) [45] were obtained for the body posture along the X, Y and Z axes, beats per minute, N-N intervals, step count, blood pressure and body temperature. Note the results for blood pressure ($R^2 = 0.9981$ and RMSE = 0.0013) and body temperature ($R^2 = 0.9942$ and RMSE = 0.0032). A low to good relationship ($R^2 > 0.25$ and $R^2 < 0.75$) [45] was obtained for the angular rate along the X, Y and Z coordinates and ECG signal, showing a trend consistent with the results obtained in the training phase. No statistically significant differences were found ($p > 0.05$) in any of the analyzed cases.

Finally, for the test dataset of the robot-assisted microsurgery sessions developed with the Symani® robotic surgical platform, Table 3 reports the values of the R^2 and RMSE derived from the application of the predictive models generated previously on the training dataset in order to externally validate them. The predictive performance is shown for the application of the CNN, MLP, MLR, RF, SVM, and UNET as predictive techniques and scaling and combined scaling and normalization as pre-processing techniques. Consistent with the results obtained on the training dataset and cross-validation, the best combination was MLR as an AI technique and scaling as a pre-processing technique, achieving the highest values of the R^2 coefficient and the lowest RMSE, followed by the SVM, RF, MLP, CNN and UNET.

The results are consistent with the training dataset and cross-validation analysis according to the criteria proposed by Colton [45]. High to excellent correlation close to 1 ($R^2 > 0.75$) and RMSE close to 0 (RMSE < 0.05) were achieved for the body posture along the X, Y and Z axes, ECG signal, beats per minute, N-N intervals, blood pressure and body temperature. The R^2 coefficient values for blood pressure ($R^2 = 0.9986$ and RMSE = 0.0011) and body temperature ($R^2 = 0.9948$ and RMSE = 0.0027) were particularly notable. A low to good relationship ($R^2 > 0.25$ and $R^2 < 0.75$) [45] was achieved for the angular rate along the X, Y and Z coordinates and step count. No statistically significant differences were found in any of the analyzed cases ($p > 0.05$).

The following table displays the results obtained for the training dataset for the robot-assisted laparoscopic surgery sessions performed by the Versius® robotic surgical platform (CMR surgical). Table 4 reports the values of the R^2 coefficient and RMSE of the training dataset for the data analysis carried out by applying the CNN, MLP, MLR, RF, SVM, and UNET as AI techniques with the dataset pre-processed by scaling and combined scaling and normalization techniques. The best performance was obtained by the combination of MLR as a predictive technique and scaling as a pre-processing technique, achieving the highest values of the R^2 coefficient and lowest RMSE. This is followed in descending order of performance by the SVM, RF, MLP, CNN and UNET.

Overall, the results achieved for the training dataset of robot-assisted laparoscopy surgery were satisfactory according to the rules given by Colton [45]. High to excellent correlation close to 1 ($R^2 > 0.75$) together with RMSE close to 0 (RMSE < 0.05) was observed for the body posture along the X, Y and Z coordinates; angular rate along the Y and Z axes; ECG signal; beats per minute; N-N intervals; step count; blood pressure and body temperature. Particularly noteworthy results were obtained for the R^2 coefficient values for blood pressure ($R^2 = 0.9982$ and RMSE = 0.0012), body temperature ($R^2 = 0.9996$ and RMSE = 0.0073) and body posture on the X coordinate ($R^2 = 0.9967$ and RMSE = 0.0108). A low to good relationship ($R^2 > 0.25$ and $R^2 < 0.75$) was exhibited for the remaining parameters analyzed.

Table 3. Results of the R^2 coefficient and RMSE for the test dataset of the ECG parameters as a function of the predictive techniques (CNN, MLP, MLR, RF, SVM, and UNET) and the pre-processing techniques (scaling and combined scaling and normalization) by using the Symani® robotic surgical platform. The best results are highlighted in bold.

		MLP		MLR		SVM		CNN		RF		UNET	
		Scaling	Scaling and Normalization	Scaling	Scaling and Normalization	Scaling	Scaling and Normalization	Scaling	Scaling and Normalization	Scaling	Scaling and Normalization	Scaling	Scaling and Normalization
Body posture X	R^2	0.8014	0.8013	**0.9078**	0.9069	0.9052	0.9036	0.6015	0.6014	0.8515	0.8514	0.4016	0.4014
	RMSE	0.1071	0.7206	**0.0385**	0.2792	0.0415	0.4632	0.3072	0.9207	0.0712	0.5206	0.5073	1.1208
Body posture Y	R^2	0.8141	0.8057	**0.9097**	0.9018	0.8973	0.8971	0.6142	0.6058	0.8642	0.8558	0.4143	0.4059
	RMSE	0.0533	0.3193	**0.0421**	0.2498	0.0506	0.2575	0.2534	0.5194	0.0523	0.2931	0.4535	0.7195
Body posture Z	R^2	0.9762	0.9471	**0.9864**	0.9846	0.9784	0.9733	0.7622	0.7470	0.9773	0.9572	0.4623	0.5471
	RMSE	0.0531	0.2375	**0.0244**	0.1095	0.0341	0.1528	0.2532	0.4376	0.0431	0.1875	0.4533	0.6377
Angular rate X	R^2	0.5219	0.5217	**0.5527**	0.5516	0.5416	0.5311	0.3221	0.3218	0.5269	0.5272	0.1222	0.1219
	RMSE	0.0371	0.5602	**0.0109**	0.1654	0.0231	0.4857	0.2372	0.7604	0.0271	0.5206	0.4373	0.9605
Angular rate Y	R^2	0.6482	0.6476	**0.7446**	0.7442	0.6959	0.6957	0.4484	0.4477	0.6628	0.6764	0.2485	0.2478
	RMSE	0.0489	0.4426	**0.0214**	0.3282	0.0357	0.3982	0.2491	0.6427	0.0419	0.4262	0.4492	0.8428
Angular rate Z	R^2	0.5097	0.5095	**0.6014**	0.5987	0.5543	0.5510	0.3098	0.3096	0.5297	0.5359	0.1099	0.1097
	RMSE	0.0198	0.5275	**0.0071**	0.1874	0.0167	0.4461	0.2199	0.7276	0.0178	0.4751	0.4201	0.9277
ECG signal	R^2	0.5431	0.5326	**0.7731**	0.7541	0.6896	0.5931	0.3432	0.3327	0.5913	0.5862	0.1434	0.1328
	RMSE	0.0198	0.6511	**0.0088**	0.3241	0.0188	0.6178	0.2108	0.8512	0.0189	0.6312	0.4109	1.0513
Beats per minute	R^2	0.7404	0.7401	**0.7541**	0.7535	0.7417	0.7413	0.5405	0.5402	0.7414	0.7411	0.3404	0.3403
	RMSE	0.0913	0.7447	**0.0436**	0.3561	0.0755	0.6161	0.2914	0.9478	0.0831	0.7247	0.4915	1.1479
N-N intervals	R^2	0.7289	0.7283	**0.8107**	0.8101	0.7974	0.7972	0.5291	0.5284	0.7798	0.7738	0.3292	0.3285
	RMSE	0.0811	0.6554	**0.0666**	0.3547	0.0692	0.5611	0.2812	0.8555	0.0781	0.5854	0.4813	1.0556
Step count	R^2	0.7111	0.7101	**0.7471**	0.7451	0.7337	0.7333	0.5112	0.5102	0.7212	0.7201	0.3113	0.3104
	RMSE	0.0447	0.3902	**0.0222**	0.1936	0.0398	0.3469	0.2448	0.5903	0.0417	0.3702	0.4449	0.7904
Blood pressure	R^2	0.9963	0.9869	**0.9986**	0.9951	0.9981	0.9916	0.7964	0.7867	0.9973	0.9889	0.5965	0.5868
	RMSE	0.0026	0.0129	**0.0011**	0.0038	0.0017	0.0075	0.2027	0.2130	0.0022	0.0092	0.4028	0.4131
Body temperature	R^2	0.9909	0.9653	**0.9948**	0.9797	0.9936	0.9728	0.7911	0.7654	0.9919	0.9683	0.5912	0.5655
	RMSE	0.0063	0.0256	**0.0027**	0.0108	0.0033	0.0141	0.2064	0.2257	0.0048	0.0206	0.4065	0.4259

Table 4. Results of the R^2 coefficient and RMSE for the training dataset of the ECG parameters as a function of the predictive techniques (CNN, MLP, MLR, RF, SVM and UNET) and the pre-processing techniques (scaling and combined scaling and normalization) by using the Versius® robotic surgical platform. The best results are highlighted in bold.

		MLP		**MLR**		**SVM**		**CNN**		**RF**		**UNET**	
		Scaling	**Scaling and Normalization**	**Scaling**	**Scaling and Normalization**	**Scaling**	**Scaling and Normalization**	**Scaling**	**Scaling and Normalization**	**Scaling**	**Scaling and Normalization**	**Scaling**	**Scaling and Normalization**
Body posture X	R^2	0.9946	0.9942	**0.9967**	0.9963	0.9954	0.9951	0.7947	0.7943	0.9951	0.9947	0.5948	0.5944
	RMSE	0.0291	0.1087	**0.0108**	0.0863	0.0174	0.1045	0.2292	0.3088	0.0241	0.1037	0.4293	0.5089
Body posture Y	R^2	0.9421	0.9418	**0.9622**	0.9609	0.9482	0.9462	0.7422	0.7419	0.9426	0.9423	0.5421	0.5418
	RMSE	0.0629	0.3432	**0.0273**	0.0348	0.0473	0.2581	0.2631	0.5434	0.0679	0.3382	0.4631	0.7435
Body posture Z	R^2	0.9093	0.9072	**0.9287**	0.9278	0.9129	0.9101	0.7094	0.7073	0.9098	0.9077	0.5095	0.5072
	RMSE	0.0705	0.4371	**0.0357**	0.2273	0.0443	0.2744	0.2707	0.6372	0.0755	0.4421	0.4708	0.8373
Angular rate X	R^2	0.6824	0.6821	**0.7044**	0.7039	0.6924	0.6904	0.4825	0.4822	0.6829	0.6826	0.2826	0.2821
	RMSE	0.1087	0.6426	**0.0377**	0.4702	0.0872	0.5584	0.3088	0.8427	0.1137	0.6476	0.5088	1.0428
Angular rate Y	R^2	0.7923	0.7919	**0.8757**	0.8748	0.8687	0.8678	0.5924	0.5921	0.7928	0.7924	0.3925	0.3920
	RMSE	0.0763	0.6432	**0.0587**	0.2494	0.0601	0.2646	0.2764	0.8433	0.0813	0.6482	0.4765	1.0433
Angular rate Z	R^2	0.7045	0.7041	**0.8905**	0.8898	0.8259	0.8255	0.5046	0.5042	0.7051	0.7046	0.3047	0.3043
	RMSE	0.0792	0.6174	**0.0234**	0.3857	0.0604	0.4296	0.2793	0.8176	0.0842	0.6224	0.4794	1.0177
ECG signal	R^2	0.6907	0.6901	**0.8076**	0.8071	0.7128	0.7124	0.4908	0.4902	0.6912	0.6906	0.2909	0.2903
	RMSE	0.1007	0.6481	**0.0816**	0.5258	0.0834	0.5368	0.3009	0.8482	0.1057	0.6531	0.5010	1.0483
Beats per minute	R^2	0.9819	0.9751	**0.9823**	0.9821	0.9821	0.9804	0.7818	0.7752	0.9824	0.9756	0.2819	0.2753
	RMSE	0.0731	0.2285	**0.0413**	0.1384	0.0602	0.1572	0.2732	0.4286	0.0781	0.2335	0.4733	0.6287
N-N intervals	R^2	0.9698	0.9666	**0.9839**	0.9731	0.9731	0.9728	0.7699	0.7666	0.9703	0.9671	0.5698	0.5667
	RMSE	0.0741	0.2603	**0.0451**	0.1581	0.0465	0.1835	0.2742	0.4605	0.0791	0.2653	0.4743	0.6606
Step count	R^2	0.7453	0.7451	**0.8821**	0.8802	0.8255	0.8038	0.5454	0.5451	0.7458	0.7456	0.3453	0.3450
	RMSE	0.0869	0.6533	**0.0736**	0.5534	0.0764	0.6042	0.2871	0.8533	0.0919	0.6583	0.4872	1.0534
Blood pressure	R^2	0.9966	0.9851	**0.9982**	0.9921	0.9970	0.9865	0.7967	0.7852	0.9971	0.9856	0.5968	0.5851
	RMSE	0.0025	0.0148	**0.0012**	0.0054	0.0019	0.0081	0.2026	0.2149	0.0075	0.0198	0.4027	0.4150
Body temperature	R^2	0.9852	0.9396	**0.9996**	0.9917	0.9961	0.9813	0.7854	0.7397	0.9857	0.9401	0.5855	0.5396
	RMSE	0.0096	0.0428	**0.0073**	0.0369	0.0089	0.0408	0.2097	0.2429	0.0146	0.0478	0.4098	0.4431

High to excellent correlations ($R^2 > 0.75$) [45] were also reached in the cross-validation analysis (Table 5) for the body posture along the X, Y, and Z axes, angular rate on the Y and Z coordinates, ECG signal, beats per minute, N-N intervals, step count, blood pressure and body temperature, in particular, for blood pressure ($R^2 = 0.9981$ and RMSE = 0.0013) and body temperature ($R^2 = 0.9994$ and RMSE = 0.0043) (Table 5). A low to good relationship ($R^2 > 0.25$ and $R^2 < 0.75$) was obtained for the angular rate along the X axis, in agreement with the training dataset. No statistically significant differences were found in any of the analyzed cases ($p > 0.05$).

Finally, for the independent test dataset corresponding to the robot-assisted laparoscopic surgery sessions developed with the Versius® robotic surgical platform, Table 6 reports the values of the R^2 coefficient and RMSE. To externally validate the predictive models generated on the training dataset, the analysis of prediction considered the application to the CNN, MLP, MLR, RF, SVM, and UNET as predictive techniques and scaling and combined scaling and normalization as pre-processing techniques. As in the training dataset and cross-validation analysis, the best combination was MLR as an AI technique and scaling as a pre-processing strategy, achieving the highest values of the R^2 coefficient and the lowest RMSE values, followed by the SVM, RF, MLP, CNN and UNET.

The results are consistent with those obtained for the training dataset and cross-validation analysis according to the criteria proposed by Colton [45]. High to excellent correlation close to 1 ($R^2 > 0.75$) and RMSE close to 0 (RMSE < 0.05) were achieved for the body posture along the X, Y and Z axes, angular rate along the Y axis, ECG signal, beats per minute, N-N intervals, step count, blood pressure and body temperature. The values for blood pressure ($R^2 = 0.9988$ and RMSE = 0.0009), body temperature ($R^2 = 0.9914$ and RMSE = 0.0061) and body posture along the X coordinates ($R^2 = 0.9906$ and RMSE = 0.0169) were particularly notable. A low to good relationship ($R^2 > 0.25$ and $R^2 < 0.75$) [45] was achieved for the angular rate along the X and Z coordinates. No statistically significant differences were found in any of the analyzed cases ($p > 0.05$).

Figure 5 illustrates the variation in the R^2 coefficient as a function of the pre-processing techniques (scaling and combined scaling and normalization) and the type of dataset (training, cross-validation and test) for robot-assisted microsurgery. As can be observed, the scaled datasets achieved higher values for R^2 coefficient values than the scaled and normalized datasets for all studied ECG parameters. Specifically, the results for the training dataset demonstrated the highest R^2 coefficient for angular rate along the Y coordinate, beats per minute, N-N intervals, step count and blood pressure. Note the value for blood pressure ($R^2 = 0.9987$). The remaining ECG parameters analyzed (body posture along the X, Y and Z coordinates; angular rate along the X and Z coordinates; ECG signal and body temperature) reached the highest R^2 coefficients for the test dataset, with the value for body temperature ($R^2 = 0.9948$) being particularly notable.

Figure 6 shows the variation in the R^2 coefficient as a function of the pre-processing techniques (scaling and combined scaling and normalization) and the type of dataset (training, cross-validation and test) for robot-assisted laparoscopic surgical sessions. Overall, the scaled datasets consistently achieved higher values for the R^2 coefficient than the scaled and normalized datasets for all ECG parameters. Consequently, the results for the training dataset demonstrated the highest R^2 coefficients for body posture along the X, Y and Z coordinates; angular rate along the Y and Z coordinates; ECG signal; N-N intervals and body temperature. Note the R^2 value for body temperature ($R^2 = 0.9996$) and for body posture along the X coordinate ($R^2 = 0.9967$). For the test dataset, angular rate along the X coordinate, beats per minute, step count, and blood pressure reached the highest R^2 values, with the R^2 value for blood pressure ($R^2 = 0.9988$) being particularly notable.

Table 5. Results of the R^2 coefficient and RMSE for the cross-validation of the ECG parameters as a function of the predictive techniques (CNN, MLP, MLR, RF, SVM, and UNET) and the pre-processing techniques (scaling and combined scaling and normalization) by using the Versius® robotic surgical platform. The best results are highlighted in bold.

		MLP		MLR		SVM		CNN		RF		UNET	
		Scaling	Scaling and Normalization	Scaling	Scaling and Normalization	Scaling	Scaling and Normalization	Scaling	Scaling and Normalization	Scaling	Scaling and Normalization	Scaling	Scaling and Normalization
Body posture X	R^2	0.9936	0.9934	**0.9962**	0.9958	0.9953	0.9947	0.7954	0.7948	0.9941	0.9939	0.5955	0.5949
	RMSE	0.0339	0.1258	**0.0124**	0.0448	0.0189	0.0951	0.2198	0.2915	0.0319	0.1238	0.4199	0.4914
Body posture Y	R^2	0.9384	0.9369	**0.9508**	0.9501	0.9465	0.9456	0.7466	0.7457	0.9389	0.9374	0.5467	0.5458
	RMSE	0.0699	0.3811	**0.0347**	0.0348	0.0549	0.0578	0.2594	0.2587	0.0679	0.3791	0.4595	0.4586
Body posture Z	R^2	0.8693	0.8653	**0.9147**	0.9119	0.8928	0.8926	0.6929	0.6927	0.8698	0.8658	0.4930	0.4926
	RMSE	0.0886	0.3675	**0.0401**	0.2526	0.0496	0.3079	0.2469	0.5097	0.0866	0.3655	0.4471	0.7096
Angular rate X	R^2	0.6239	0.6227	**0.6879**	0.6784	0.6388	0.6359	0.4389	0.4360	0.6244	0.6232	0.2390	0.2359
	RMSE	0.1291	1.0972	**0.0359**	0.4477	0.0873	0.8539	0.2837	1.0593	0.1271	1.0952	0.4838	1.2592
Angular rate Y	R^2	0.7475	0.7435	**0.8549**	0.8537	0.8507	0.8496	0.6508	0.6497	0.7480	0.7440	0.4509	0.4496
	RMSE	0.0833	0.7025	**0.0331**	0.2788	0.0413	0.2845	0.2431	0.4854	0.0813	0.7005	0.4432	0.6853
Angular rate Z	R^2	0.6656	0.6069	**0.8283**	0.8031	0.8081	0.7814	0.6082	0.5815	0.6661	0.6074	0.4083	0.3814
	RMSE	0.1056	1.0787	**0.0217**	0.4649	0.0588	0.4769	0.2588	0.6786	0.1036	1.0767	0.4589	0.8785
ECG signal	R^2	0.6787	0.6762	**0.8041**	0.7903	0.6998	0.6988	0.4999	0.4989	0.6792	0.6767	0.2901	0.2988
	RMSE	0.1169	0.7649	**0.0369**	0.5421	0.1156	0.5641	0.3165	0.7614	0.1149	0.7629	0.5166	0.9613
Beats per minute	R^2	0.9751	0.9719	**0.9821**	0.9819	0.9787	0.9782	0.7788	0.7783	0.9756	0.9724	0.5789	0.5782
	RMSE	0.0682	0.1856	**0.0417**	0.1398	0.0512	0.1711	0.2521	0.3711	0.0662	0.1836	0.4522	0.5709
N-N intervals	R^2	0.9637	0.9621	**0.9821**	0.9716	0.9694	0.9693	0.7695	0.7694	0.9642	0.9626	0.5696	0.5693
	RMSE	0.0819	0.2876	**0.0671**	0.1616	0.0741	0.1809	0.2714	0.3891	0.0799	0.2856	0.4741	0.5819
Step count	R^2	0.6724	0.6704	**0.8746**	0.8226	0.7281	0.7275	0.5282	0.5276	0.6729	0.6709	0.3283	0.3275
	RMSE	0.1611	0.8276	**0.0752**	0.5614	0.1246	0.6893	0.3264	0.8839	0.1581	0.8256	0.5246	1.0893
Blood pressure	R^2	0.9958	0.9817	**0.9981**	0.9916	0.9966	0.9828	0.7967	0.7829	0.9963	0.9822	0.5968	0.5831
	RMSE	0.0032	0.0171	**0.0013**	0.0057	0.0028	0.0144	0.2082	0.2144	0.0027	0.0151	0.4028	0.4143
Body temperature	R^2	0.9981	0.9819	**0.9994**	0.9915	0.9987	0.9827	0.7988	0.7828	0.9986	0.9824	0.5987	0.5829
	RMSE	0.0139	0.0473	**0.0043**	0.0386	0.0078	0.0459	0.2087	0.2495	0.0119	0.0453	0.4078	0.4259

Table 6. Results of the R^2 coefficient and RMSE for the test dataset of the ECG parameters as a function of the predictive techniques (CNN, MLP, MLR, RF, SVM, and UNET) and the pre-processing techniques (scaling and combined scaling and normalization) by using the Versius® robotic surgical platform. The best results are highlighted in bold.

		MLP		**MLR**		**SVM**		**CNN**		**RF**		**UNET**	
		Scaling	**Scaling and Normalization**	**Scaling**	**Scaling and Normalization**	**Scaling**	**Scaling and Normalization**	**Scaling**	**Scaling and Normalization**	**Scaling**	**Scaling and Normalization**	**Scaling**	**Scaling and Normalization**
Body posture X	R^2	0.9863	0.9849	**0.9906**	0.9902	0.9528	0.9519	0.7582	0.7591	0.9868	0.9854	0.4584	0.4593
	RMSE	0.0438	0.0638	**0.0169**	0.0531	0.0209	0.0784	0.2291	0.2748	0.0428	0.0628	0.4219	0.4747
Body posture Y	R^2	0.7561	0.7558	**0.8457**	0.8454	0.7854	0.7756	0.5845	0.5765	0.7566	0.7563	0.3847	0.3767
	RMSE	0.0913	0.9709	**0.0637**	0.3473	0.0797	0.6284	0.2779	0.8248	0.0903	0.9699	0.4781	1.0247
Body posture Z	R^2	0.8574	0.8571	**0.9267**	0.9261	0.8853	0.8848	0.6835	0.6848	0.8579	0.8576	0.4838	0.4851
	RMSE	0.0833	0.5168	**0.0465**	0.2886	0.0581	0.3598	0.2518	0.5589	0.0823	0.5158	0.4528	0.7591
Angular rate X	R^2	0.6516	0.6511	**0.7198**	0.7192	0.7125	0.7046	0.5152	0.5064	0.6521	0.6516	0.3154	0.3066
	RMSE	0.0793	0.4456	**0.0274**	0.3417	0.0517	0.3795	0.2571	0.5759	0.0783	0.4446	0.4571	0.7761
Angular rate Y	R^2	0.6425	0.6372	**0.7516**	0.7505	0.7468	0.7456	0.5486	0.5465	0.6430	0.6377	0.3484	0.3463
	RMSE	0.0926	0.7807	**0.0351**	0.2961	0.0873	0.4168	0.2837	0.6186	0.0916	0.7796	0.4837	0.8186
Angular rate Z	R^2	0.5791	0.5783	**0.6383**	0.6381	0.6242	0.6136	0.4224	0.4163	0.5796	0.5788	0.2224	0.2163
	RMSE	0.0618	1.0171	**0.0528**	0.4446	0.0589	0.8049	0.2598	1.0094	0.0608	1.0161	0.4598	1.2093
ECG signal	R^2	0.7436	0.7433	**0.7974**	0.7952	0.7332	0.7329	0.5324	0.5392	0.7441	0.7438	0.3324	0.3392
	RMSE	0.1038	0.6685	**0.0672**	0.4329	0.0735	0.5735	0.2753	0.7753	0.1028	0.6675	0.4754	0.9735
Beats per minute	R^2	0.9671	0.9663	**0.9842**	0.9813	0.9694	0.9692	0.7649	0.7629	0.9676	0.9668	0.5649	0.5629
	RMSE	0.0873	0.2623	**0.0423**	0.1417	0.0637	0.2131	0.2673	0.4114	0.0863	0.2613	0.4674	0.6214
N-N intervals	R^2	0.9418	0.9316	**0.9698**	0.9688	0.9649	0.9647	0.7694	0.7674	0.9423	0.9321	0.5694	0.5674
	RMSE	0.0671	0.2355	**0.0481**	0.1588	0.0583	0.2048	0.2538	0.4084	0.0661	0.2345	0.4538	0.6184
Step count	R^2	0.7585	0.6592	**0.9068**	0.8066	0.8169	0.7136	0.6196	0.5163	0.7590	0.6597	0.4196	0.3163
	RMSE	0.1922	1.4487	**0.0654**	0.4918	0.1186	0.8928	0.3168	1.0982	0.1912	1.4477	0.5169	1.2984
Blood pressure	R^2	0.9953	0.9794	**0.9988**	0.9945	0.9972	0.9819	0.7927	0.7891	0.9958	0.9799	0.5927	0.5891
	RMSE	0.0031	0.0139	**0.0009**	0.0042	0.0026	0.0075	0.2062	0.2057	0.0021	0.0129	0.4063	0.4058
Body temperature	R^2	0.9859	0.9429	**0.9914**	0.9525	0.9867	0.9466	0.7876	0.7466	0.9864	0.9434	0.5878	0.5464
	RMSE	0.0091	0.0404	**0.0061**	0.0267	0.0076	0.0342	0.2067	0.2324	0.0081	0.0394	0.4067	0.4325

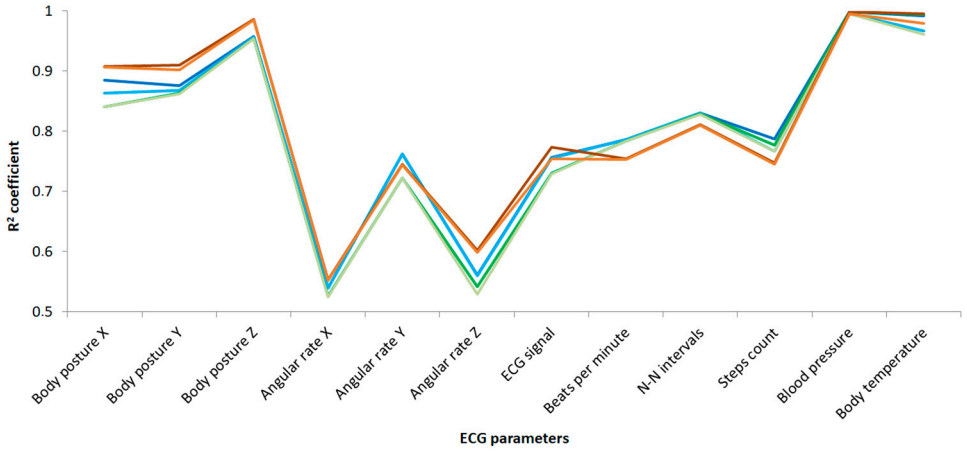

Figure 5. Results for the R^2 coefficient values for robot-assisted microsurgery, applying MLR as a predictive technique as a function of the following groups: training dataset and scaling (dark blue), training dataset and scaling and normalization (light blue), cross-validation and scaling (dark green), cross-validation and scaling and normalization (light green), test dataset and scaling (dark orange) and test dataset and scaling and normalization (light orange).

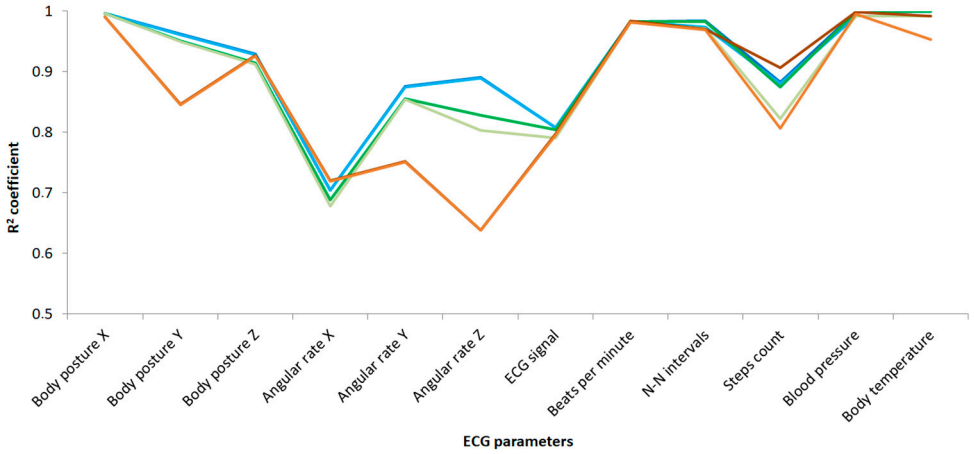

Figure 6. Results for the R^2 coefficient values for robot-assisted laparoscopy surgery, applying MLR as a predictive technique as a function of the following groups: training dataset and scaling (dark blue), training dataset and scaling and normalization (light blue), cross-validation and scaling (dark green), cross-validation and scaling and normalization (light green), test dataset and scaling (dark orange) and test dataset and scaling and normalization (light orange).

Figure 7 illustrates the correlation between the results estimated by applying AI, for classification into three categories (0: low stress level; 1: medium stress level; and 2: high stress level) and the results reported from the stress survey by the surgeons after the microsurgical activity. The rates for the original survey were between 0 and 10, but they were categorized as: 0: low stress level (0–3 on the survey); 1: medium stress level (4–7 on the survey); and 2: high stress level (8–10 on the survey).

Two surgeons reported a low level of stress in the questionnaire. In this case, the prediction model classified both cases with a medium stress level. Seven surgeons reported a medium stress level, among which the predictive model established a medium stress level for three of them and a high stress level for the remaining four surgical sessions. Finally, three surgeons reported a high stress level in the survey, and all of them were correctly classified with a high stress level by the predictive model. Therefore, six of twelve robot-assisted microsurgical sessions were correctly classified, yielding the R^2 coefficient of 0.7989.

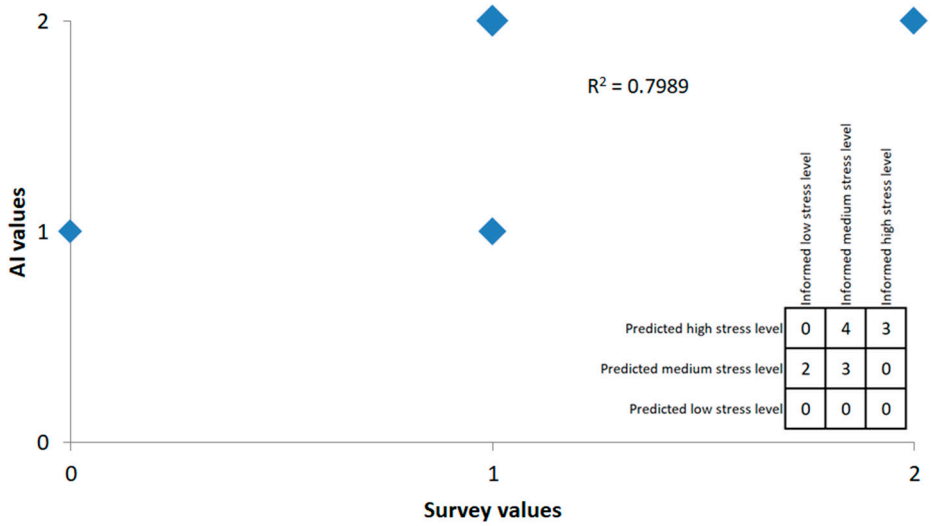

Figure 7. Correlation between values obtained from the stress feeling surveys and the values predicted by applying AI during robot-assisted microsurgical activities. The confusion matrix is presented in the lower right part of the figure.

Figure 8 displays the correlation between the results estimated by applying AI for classification into three categories of stress levels (0: low stress level; 1: medium stress level; and 2: high stress level) and the results reported from the stress-sensitive questionnaire by the surgeons after the robot-assisted laparoscopy surgical activity. The rates for the survey ranged between 0 and 10, but they were evaluated for the current study as: 0: low stress level (0–3 on the survey); 1: medium stress level (4–7 on the survey); and 2: high stress level (8–10 on the survey). Seven surgeons reported a low stress level in the survey. Among these cases, the predictive model classified five of them correctly with a low stress level and misclassified two cases with a medium stress level. Six surgeons reported a medium stress level, for which the predictive model established a low stress level for the remaining one. Finally, one surgeon reported a high stress level in the questionnaire, and all of them were correctly classified with a high stress level by the predictive model. Therefore, ten of fourteen surgical sessions were correctly classified, and the obtained R^2 coefficient value was 0.8381.

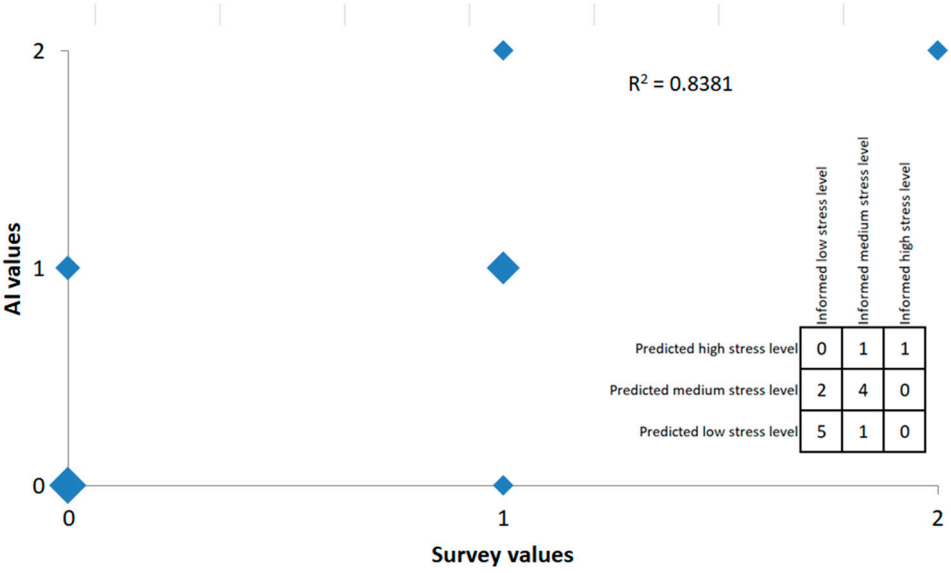

Figure 8. Correlation between values obtained from the stress feeling surveys and the values predicted by applying AI during robot-assisted laparoscopy activities. The confusion matrix is presented in the lower right part of the figure.

4. Discussion

On one hand, the results observed for the training dataset are satisfactory according to the criteria proposed by Colton [45]. High to excellent correlation close to 1 ($R^2 > 0.75$) and RMSE close to 0 (RMSE < 0.05) was reached for most ECG parameters analyzed. However, the attributes related to the surgeon's ergonomic (angular rate along the X and Z coordinates) exhibited lower correlation ($R^2 < 0.75$), which could be related to the surgeon's surgical experience and the stress level generated during the performance of the surgical activities [47].

The results achieved were lower than those obtained with the training dataset. Nevertheless, the results observed were satisfactory as far as the training dataset is concerned. High to excellent correlations ($R^2 > 0.75$) [45] were reached for most ECG parameters analyzed. However, the attributes are those related to the surgeon's ergonomic and ECG sensor (angular rate on the X, Y and Z coordinates and ECG signal) exhibited lower correlation ($R^2 < 0.75$), similar to the training, which could be related to the surgeon's surgical experience and the stress level generated during surgical activities [47].

The results were consistent with the results obtained on the training dataset. High to excellent correlation close to 1 ($R^2 > 0.75$) [45] and RMSE close to 0 (RMSE < 0.05) were achieved for the body posture along the X, Y and Z coordinates; ECG signal; beats per minute; N-N intervals; blood pressure and body temperature. A low to good relationship ($R^2 > 0.25$ and $R^2 < 0.75$) [45] was achieved for the attributes related to the surgeon's ergonomic and kinematic metrics (angular rate on the X, Y and Z coordinates and step count), which could be related to the surgeon's surgical experience and the stress levels generated during surgical activities [47].

To the best of our knowledge, there are no scientific studies applying ECG sensor data to microsurgery in order to measure stress levels. However, D'ambrosia et al. [48] analyzed the operator performance on RAS and microsurgery simulations by using electrocardiogram (ECG) sensors, showing similar values of error (RMSE < 0.01). Additionally, D'ambrosia et al. [48] indicated the use of some additional sensors such as electroencephalogram (EEG) devices. In the same way, some studies analyzed stress level based only on the heart rate variability [49,50].

On other hand, the results achieved for the training dataset of robot-assisted laparoscopy surgery were satisfactory. High to excellent correlation close to 1 ($R^2 > 0.75$) [45] and RMSE close to 0 (RMSE < 0.05) were obtained for the body posture along the X, Y and Z coordinates; angular rate Y and Z coordinates; ECG signal; beats per minute; N-N intervals; blood pressure and body temperature. A low to good relationship ($R^2 > 0.25$ and $R^2 < 0.75$) [45] was achieved for the other parameters analyzed. The remaining attributes are those related to the surgeon's kinematic parameters (angular rate on the X coordinate) and step count, which could be related to the surgeon's surgical experience and the stress levels generated during the performance of surgical activities [47].

The results achieved in robot-assisted laparoscopy surgery were lower than those obtained with the training dataset. Nevertheless, the results obtained are notable as far as the training dataset is concerned. High to excellent correlations ($R^2 > 0.75$) [45] were reached for the body posture along the X, Y and Z coordinates and ECG signal, these being attributes related to the surgeon's kinematic parameters; these results are similar to those obtained from the training dataset, and this fact could be related to the variability in the surgeon's surgical experience and the stress generated during surgical activities [47].

The results with the Versius® robotic platform were similar to the training dataset. High to excellent correlation close to 1 (R2 > 0.75) [45] and RMSE close to 0 (RMSE < 0.05) were achieved for the body posture along the X, Y and Z coordinates; angular rate along the Y coordinate; ECG signal; beats per minute; N-N intervals; step count; blood pressure and

body temperature. A low to good relationship ($R^2 > 0.25$ and $R^2 < 0.75$) [45] was achieved for the attributes related to the surgeon's kinematic parameters (angular rate along the X and Z coordinates), which could be related to the variability in the surgeon's surgical experience and the stress generated during surgical activities [47].

In comparison to previous studies, an ECG sensor was used throughout the robot-assisted laparoscopy surgery for measuring physiological stress during surgery [51]. This study reported that robot-assisted laparoscopy achieved lower heart rate variability and lower stress level than the conventional method. As in previous study [48], expert surgeons are well adapted to this type of stress [52] due to their previous experience. This fact shows that most of the surgeons reach extreme heart rate variability and high stress levels in comparison to general physicians [53].

Considering the results obtained in Figure 5, any pre-processing technique could be performed. Nevertheless, the slightly better results achieved for the scaling pre-processing technique indicated that it would be the optimal pre-processing technique in this case. In general, the results obtained with the Symani® robotic platform, focused on microsurgery, involved minimal movements by the surgeon; consequently, the ECG parameters related to the surgeon's ergonomic and kinematic metrics achieved lower R^2 coefficients since the variability in these values was very high. These results were in agreement with the results achieved in previous studies [54]. These minimal movements by the surgeon and some ECG parameters related to heart rate also achieved lower R^2 coefficients due to the variability in these values [54].

In the case of Figure 6, as well as the robot-assisted microsurgical activities, any pre-processing technique could be performed, although the slightly better results observed for the scaling pre-processing technique specified that it would be the optimal pre-processing technique. Overall, the results obtained with the Versius® robotic surgery platform, focused on robot-assisted laparoscopy surgery, entailed a greater range of motion by the surgeon and, consequently, the ECG parameters related to the surgeon's ergonomic and kinematic metrics achieved lower R^2 coefficients since the variability in these values is very high. However, these R^2 coefficients were higher than those of the robot-assisted microsurgery. The results were in agreement with the results achieved in previous studies [54]. Consequently, the results from Figures 5 and 6 are consistent with the use of each robotic surgery platform [54].

The results obtained for Figure 7 are a good starting point for the evolution of the current AI model ($R^2 = 0.7989$) for improving the results obtained in future iterations, with it also being necessary to test and to check different models based on CNNs and DLMs.

Some studies have been analyzed in order to measure and quantify the stress level of surgeons during microsurgical activities, showing slightly lower R^2 coefficients for all cases. However, in those studies, the stress was not measured as a function of the attributes of the ECG sensor. As example, Carr et al. [55] measured the effect of stress on anastomosis carried out by plastic surgeons. Fourteen surgeons participated in the study (six novices and eight experts), with two sessions by surgeons (twenty-eight total sessions). The correlation coefficient for the novice surgeons was 0.71 ($R^2 = 0.5041$), and 0.88 was the correlation coefficient for the expert surgeons ($R^2 = 0.7744$), both values being lower than the value obtained in our study ($R^2 = 0.7989$) for the microsurgery activities, confirming the good results obtained in the current study.

For the development of robot-assisted laparoscopy surgery (Figure 8) the obtained results were superior to the results obtained for the microsurgical activities (Figure 7). The current study is considered a promising point to start the evolution of the current AI model. The extensive use of CNN or DLM models and increasing the number of algorithms

evaluated and compared would be interesting future developments in order to improve the current AI model.

Some studies on robot-assisted laparoscopy surgery activities have been analyzed in order to measure and to quantify the stress level of the surgeons, showing slightly lower R^2 coefficients for all cases. As example, Heemskerk et al. [51] showed that the RAS achieved lower stress levels than the conventional robot-assisted laparoscopy surgery; however, that study showed that the maximum stress level for the surgeons is not known. Fourteen surgical sessions were performed by two surgeons, and nine of them were correctly classified between the subjective and objective stress level, and the remaining five were incorrectly classified, achieving slightly worse classification than our study that classified ten of them correctly and four of them incorrectly.

The use of the data from stress-sensitive surveys presents a limitation since this data is subjective for each surgeon. For further studies, the use of a new objective index based on the parameters obtained from the ECG sensor could be adopted. In the same way, in further studies the number of surgeons and surgery sessions should be increased in order to reinforce the evidence of the presented results.

In future developments, the enhanced predictive models could be incorporated into real-time monitoring platforms to support systems capable of suggesting or scheduling appropriate rest periods for surgeons. Such tools could contribute to reducing the risk of long-term health issues while also supporting better surgical performance and overall procedure quality. In addition, the optimization of each applied algorithm should be developed in order to provide the optimal hyperparameters necessary in each case study. Finally, additional categorization of the data by surgeon, task or surgical session should also be tested in order to obtain more conclusive results.

5. Conclusions

A novel predictive model based on a linear approach (MLR) was developed to estimate some physiological, kinematic and ergonomic attributes during the surgeon's surgical performance in RAS. This model achieved high R^2 coefficients ($R^2 > 0.75$) and low values of error (RMSE < 0.05) for most parameters but an angular rate on some coordinates and ECG.

Considering the pre-processing techniques evaluated in the current study, scaling achieved, in general, higher R^2 coefficients and lower error ($R^2 > 0.75$ and RMSE < 0.05) than scaling and normalization. Consequently, the best combination for predicting the stress levels of the surgeon during RAS activities, using both robotic platforms for laparoscopy surgery and microsurgery, was MLR as an AI technique and scaling as a pre-processing technique.

The results observed by applying the AI model were compared to the stress feeling surveys completed by the surgeons about stress levels during the performance of RAS activities. The same results were obtained in six of the twelve surgical sessions for the microsurgery activities. Therefore, this is a good and promising starting point for predicting the surgeon's stress when performing RAS and demonstrates the option to predict factors that help us to enhance the surgeon's health during RAS.

Author Contributions: Conceptualization, D.C., M.J.P.-S., J.A.S.-M. and F.M.S.-M.; methodology, D.C., M.J.P.-S., J.A.S.-M. and F.M.S.-M.; software, D.C., M.J.P.-S. and J.A.S.-M.; validation, D.C., M.J.P.-S., J.A.S.-M. and F.M.S.-M.; formal analysis, D.C., M.J.P.-S., J.A.S.-M. and F.M.S.-M.; investigation, D.C., M.J.P.-S., J.A.S.-M. and F.M.S.-M.; resources, D.C., M.J.P.-S., J.A.S.-M. and F.M.S.-M.; data curation, D.C., M.J.P.-S. and J.A.S.-M.; writing—original draft preparation, D.C., M.J.P.-S. and J.A.S.-M.; writing—review and editing, D.C., M.J.P.-S., J.A.S.-M. and F.M.S.-M.; visualization, D.C., M.J.P.-S. and J.A.S.-M.; supervision, J.A.S.-M. and F.M.S.-M.; project administration, D.C., M.J.P.-S.,

J.A.S.-M. and F.M.S.-M.; funding acquisition, J.A.S.-M. and F.M.S.-M. All authors have read and agreed to the published version of the manuscript.

Funding: This work was financed by the Ministry of Science and Innovation with funds from the European Union Next Generation EU, from the Recovery, Transformation and Resilience Plan (PRTR-C17.I1), the Junta de Extremadura (GR24210), and the European Regional Development Fund (ERDF) of Extremadura Operational Program 2021–2027.

Institutional Review Board Statement: Not applicable.

Informed Consent Statement: Informed consent was obtained from all subjects involved in the study.

Data Availability Statement: Data are available on request due to restrictions, e.g., privacy or ethics.

Acknowledgments: The authors would like to thank the colleagues who collaborated in this study.

Conflicts of Interest: The authors declare no conflict of interest.

Abbreviations

The following abbreviations are used in this manuscript:

ECG	Electrocardiogram
RAS	Robot-Assisted Surgery
AI	Artificial Intelligence
MLR	Multiple Linear Regression
CNN	Convolutional Neural Network
DLM	Deep Learning Methods
SVM	Support Vector Machine
ANN	Artificial Neural Network
MLP	Multilayer Perceptron
RMSE	Root Mean Square Error

References

1. Hurley, A.M.; Kennedy, P.J.; O'Connor, L.; Dinan, T.G.; Cryan, J.F.; Boylan, G.; O'Reilly, B. SOS save our surgeons: Stress levels reduced by robotic surgery. *Gynecol. Surg.* **2015**, *12*, 197–206. [CrossRef]
2. Ballantyne, G.H. Robotic surgery, telerobotic surgery, telepresence, and telementoring. Review of early clinical results. *Surg. Endosc.* **2002**, *16*, 1389–1402. [CrossRef]
3. Berguer, R.; Forkey, D.; Smith, W. Ergonomic problems associated with laparoscopic surgery. *Surg. Endosc.* **1999**, *13*, 466–468. [CrossRef]
4. Kaplan, J.R.; Lee, Z.; Eun, D.D.; Reese, A.C. Complications of Minimally invasive surgery and their management. *Curr. Urol. Rep.* **2016**, *17*, 47. [CrossRef] [PubMed]
5. Pehlivanoglu, B.; Durmazlar, N.; Balkanci, D. Computer adapted stroop color-word conflict test as a laboratory stress model. *Erciyes Med. J.* **2005**, *27*, 58–63.
6. Chang, Y.; He, C.; Tsai, B.Y.; Ko, L.W. Multi-parameter physiological state monitoring in target detection under real world settings. *Front. Hum. Neurosci.* **2021**, *15*, 785562. [CrossRef]
7. Klein, M.I.; Warm, J.S.; Riley, M.A. Mental workload and stress perceived by novice operators in the laparoscopic and robotic minimally invasive surgical interfaces. *J. Endourol.* **2012**, *26*, 1089–1094. [CrossRef]
8. Nath, R.K.; Thpliyal, H.; Caban-Holt, A.; Mohanty, S.P. Machine learning based solutions for real time stress monitoring. *IEEE Consum. Electron. Mag.* **2020**, *9*, 34–41. [CrossRef]
9. Arora, S.; Sevdalis, N.; Nestel, D.; Woloshynowych, M.; Darzi, A.; Kneebone, R. The impact of stress on surgical performance: A systematic review of the literature. *Surgery* **2010**, *147*, 311–330. [CrossRef]
10. Saoughi, F.; Behmanesh, A.; Sayfouri, N. Internet of things in medicine: A systematic mapping study. *J. Biomed. Inform.* **2020**, *103*, 103383. [CrossRef] [PubMed]
11. Hickey, B.A.; Chalmers, T.; Newton, P.; Lin, C.T.; Sibbritt, D.; McLachlan, C.S.; Clifton-Bligh, R.; Morley, J.; Lal, S. Smart devices and wearable technologies to detect and monitor mental health conditions and stress: A systematic review. *Sensors* **2021**, *21*, 3461. [CrossRef]

12. Zangroniz, R.; Martínez-Rodrigo, A.; Pastor, J.M.; López, M.T.; Fernández-Caballero, A. Electrodermal activity sensor for classification of calm/distress condition. *Sensors* **2017**, *17*, 2324. [CrossRef]
13. Tulen, H.M.; Moleman, P.; Steenist, H.G.V.; Boomsma, F. Characterization of stress reactions to the stroop color word test. *Pharmacol. Biochem. Behav.* **1989**, *32*, 9–15. [CrossRef]
14. Hjortskov, N.; Rissen, D.; Blangsted, A.K.; Fallentin, N.; Lundberg, U.; Sogaard, K. The effect of mental stress on heart rate variability and blood pressure during computer work. *Eur. J. Appl. Physiol.* **2004**, *92*, 84–89. [CrossRef]
15. Linden, W. What do arithmetic stress measure? Protocol variation and cardiovascular response. *J. Psychophysiol.* **1991**, *28*, 91–102. [CrossRef]
16. Hwang, M.; Ichonowski, J.; Thananjeyanm, B.; Seita, D.; Paradis, S.; Fer, D.; Low, T.; Goldberg, K. Automating surgical peg transfer: Calibration with deep learning can exceed speed, accuracy, and consistency of humans. *IEEE Trans. Autom. Sci. Eng.* **2022**, *20*, 909–922. [CrossRef]
17. Shi, W.; Liu, P.X.; Zheng, M. Cutting procedures with improved visual effects and haptic interaction for surgical simulation systems. *Comput. Methods Program. Biomed.* **2020**, *184*, 105270. [CrossRef] [PubMed]
18. Phan, P.T.; Honag, T.T.; Thai, M.T.; Low, H.; Davies, J.; Lovell, N.H.; Do, T.N. Smart surgical sutures using soft artificial muscles. *Sci. Rep.* **2021**, *11*, 22420. [CrossRef]
19. Healey, J.A.; Picard, R.W. Detecting stress during real-world driving tasks using physiological sensors. *IEEE Intell. Trans. Syst.* **2005**, *6*, 156–166. [CrossRef]
20. Ávila-Tomás, J.F.; Mayer-Pujadas, M.A.; Quesada-Varela, V.J. La inteligencia artificial y sus aplicaciones en medicina I: Introducción y antecedentes a la IA y robótica. *Aten. Primaria* **2020**, *52*, 778–784. [CrossRef] [PubMed]
21. Janiesch, C.; Zschech, P.; Heinrich, K. Machine learning and deep learning. *Electron. Mark.* **2021**, *31*, 685–695. [CrossRef]
22. Greene, S.; Thapliyal, H.; Cabn-Holt, A. A survey of affective computing for stress detection. Evaluating technologies in stress detection for better health. *IEEE Consum. Electron. Mag.* **2016**, *5*, 44–56. [CrossRef]
23. Smets, E.; Raedt, W.D.; Hoof, C.V. Into the wild: The challenges of physiological stress detection in laboratory and ambulatory settings. *IEEE J. Biomed. Health Inform.* **2018**, *23*, 463–473. [CrossRef]
24. Trunfio, T.A.; Scala, A.; Giglio, C.; Rossi, G.; Borrelli, A.; Romano, M.; Improta, G. Multiple Regression model to analyze the total LOS for patients undergoing laparoscopic appendectomy. *BMC Med. Inform. Decis. Mak.* **2022**, *22*, 141. [CrossRef]
25. Gupta, R.; Alam, A.; Agarwal, P. Modified support vector machine for detecting stress level using EEG signal. *Comput. Intell. Neurosci.* **2020**, *2020*, 8860841. [CrossRef]
26. Ballabio, D.; Vasighi, M. A MATLAB toolbox for self-organizing maps and supervised neural network learning Strategies. *Chemom. Intell. Lab. Syst.* **2012**, *118*, 24–32. [CrossRef]
27. Sánchez-Margallo, J.A.; Sánchez-Margallo, F.M. Intial experience using a robotic-driven laparoscopic needle holder with ergonomic handle: Assessment of surgeons' task performance and ergonomics. *Int. J. Comput. Assist. Radiol. Surg.* **2017**, *12*, 2069–2077. [CrossRef]
28. Sánchez-Margallo, J.A.; Plaza-de-Miguel, C.; Fernández-Anzules, R.A.; Sánchez-Margallo, F.M. Application of Mixed Reality in medical training and Surgical planning focused on minimally invasive surgery. *Front. Virtual Real.* **2021**, *2*, 692641. [CrossRef]
29. Caballero, D.; Sánchez-Margallo, J.A.; Pérez-Salazar, M.J.; Sánchez-Margallo, F.M. Applications of Artificial Intelligence in Minimally Invasive Surgery Training: A scoping review. *Surgeries* **2025**, *6*, 7. [CrossRef]
30. Weenik, M.; Alken, A.P.B.; Engelen, L.J.L.P.G.; Bredje, S.J.H.; Van de Belt, T.H.; Van Goor, H. Stress measurement in surgeons and residents using a smart patch. *Am. J. Surg.* **2018**, *216*, 361–368. [CrossRef] [PubMed]
31. Siemionow, M.; Ozer, K.; Siemionow, W.; Lister, G. Robotic assistance in microsurgery. *J. Reconstr. Microsurg.* **2000**, *16*, 643–649. [CrossRef]
32. Oka, M. Interpreting a standardized and normalized measure of neighbourhood socio-economic status for a better understanding of health differences. *Arch. Public Health* **2021**, *79*, 226. [CrossRef] [PubMed]
33. Dietterich, T. Approximate statistical tests for comparing supervised classification learning algorithms. *Neural Comput.* **1998**, *10*, 1895–1923. [CrossRef] [PubMed]
34. Frank, E.; Hall, M.A.; Witten, I.H. *The WEKA Workbench*; Online Appendix for Data Mining: Practical Machine Learning Tools and Techniques; Morgan Kauffmann: Burlington, MA, USA, 2016.
35. Grossman, R.; Seni, G.; Elder, J.; Agarwal, N.; Liu, H. *Ensemble Methods in Data Mining: Improving Accuracy Through Combining Predictions*; Morgan and Claypool Publishers: Williston, VT, USA, 2010.
36. LeCunn, Y.; Bengio, Y. Convolutional networks for images, speech and time series. In *The Handbook of Brain Theory and Neural Networks*; MIT Press: Cambridge, MA, USA, 1995.
37. Wu, X.; Kumar, V.; Ross-Quinlan, J.; Ghosh, J.; Yang, Q.; Motoda, H.; McLachlan, G.J.; Ng, A.; Liu, B.; Yu, P.S.; et al. Top 10 algorithms in data mining. *Knowl. Inf. Syst.* **2008**, *14*, 1–37. [CrossRef]
38. Bishop, C.M. *Pattern Recognition and Machine Learning*; Springer: New York, NY, USA, 2006.

39. Caballero, D.; Pérez-Salazar, M.J.; Sánchez-Margallo, J.A.; Sánchez-Margallo, F.M. Optimization of an artificial neural network for predicting stress in robot-assisted laparoscopic surgery based on EDA sensor data. *Int. J. Comput. Assist. Radiol. Surg.* **2025**, *20*, 1665–1675. [CrossRef] [PubMed]
40. Fayyad, U.; Piatetsky-Shapiro, G.; Smyth, P. From data mining to knowledge discovery in databases. *Am. Assoc. Artif. Intell.* **1996**, *17*, 37–54.
41. Caballero, D.; Caro, A.; Dahl, A.B.; Ersboll, B.K.; Amigo, J.M.; Pérez-Palacios, T.; Antequera, T. Comparison of different image analysis algorithm on MRI to predict physico-chemical nad sensory attributes of loin. *Chemom. Intell. Lab. Syst.* **2018**, *180*, 54–63. [CrossRef]
42. Breiman, L. Random Forest. *Mach. Learn.* **2001**, *45*, 5–32. [CrossRef]
43. Vapnik, V.N.; Chervonenskis, Y.A. On the uniform convergence of relative frequencies of events to their probabilities. *Theory Probab.* **1971**, *16*, 264–280. [CrossRef]
44. Ronneberger, O.; Fischer, P.; Brox, T. U-Net: Convolutional networks for biomedical image segmentation. *Lect. Notes Comp. Sci.* **2015**, *9351*, 234–241.
45. Colton, T. *Statistics in Medicine*; Little Brown and Co.: New York, NY, USA, 1974.
46. Hyndman, R.; Koehler, A.B. Another look to measures of forecast accuracy. *Int. J. Forecast.* **2006**, *22*, 679–688. [CrossRef]
47. Amirthanayagam, A.; Zecca, M.; Barber, S.; Singh, B.; Moss, E. Impact of minimally invasive surgery on surgeon health (issue) study: Protocol of a single-arm observational study conducted in the live surgery setting. *BMJ Open* **2023**, *13*, e066765. [CrossRef]
48. D'ambrosia, C.; Aronoff-Spencer, E.; Huang, E.Y.; Goldhaber, N.H.; Jacobser, G.R.; Sandler, B.; Horgan, S.; Appelbaum, L.G.; Christiansen, H.; Broderick, R.C. The physiology of intraoperative error: Using electrocardiograms to understand operator performance during robot-assisted surgery simulations. *Surg. Endosc.* **2023**, *37*, 4641–4650. [CrossRef]
49. Kim, H.G.; Cheon, E.J.; Bai, D.S.; Lee, Y.H.; Koo, B.H. Stress and heart rate variability: A meta-analysis and review of the literature. *Psychiatry Investig.* **2023**, *15*, 235–245. [CrossRef] [PubMed]
50. Zhu, J.; Li, L.; Liu, C. Heart rate variability monitoring for emotion and disorders of emotion. *Physiol. Meas.* **2019**, *40*, 064004. [CrossRef]
51. Heemskerk, J.; Zandberger, H.R.; Keet, S.W.M.; Martijnse, I.; van Montfort, G.; Peters, R.J.A.; Svircevic, V.; Bouwman, R.A.; Baeten, C.G.M.I.; Bouvy, N.D. Relax, It's just laparoscopy! A prospective randomized trial on heart rate variability of the surgeon in robot-assisted versus conventional laparoscopic cholecystectomy. *Dig. Surg.* **2014**, *31*, 225–232. [CrossRef]
52. Becker, W.G.; Ellis, H.; Goldsmith, R.; Kaye, A.M. Heart rates of surgeons in theatre. *Ergonomics* **1983**, *26*, 803–807. [CrossRef]
53. Arnetz, B.B.; Andreasson, S.; Strandberg, M.; Eneroth, P.; Kallner, A. Comparison between surgeons and general practitioners with respect to cardiovascular and psychosocial risk factors among physicians. *Scand. J. Work. Environ. Health* **1988**, *14*, 118–124. [CrossRef] [PubMed]
54. Shalabi, L.A.; Shaaban, Z.; Kasasbeh, B. Data mining: A processing engine. *J. Comput. Sci.* **2006**, *2*, 735–739. [CrossRef]
55. Carr, S.; McDermott, B.R.; McInerneey, N.; Hussey, A.; Byrne, D.; Potter, S. Determining the effect of external stressors and cognitive distraction on microsurgical skills and performance. *Front. Surg.* **2020**, *6*, 77. [CrossRef]

Disclaimer/Publisher's Note: The statements, opinions and data contained in all publications are solely those of the individual author(s) and contributor(s) and not of MDPI and/or the editor(s). MDPI and/or the editor(s) disclaim responsibility for any injury to people or property resulting from any ideas, methods, instructions or products referred to in the content.